A Novel Positioning and Orientation System Based on Three-Axis Magnetic Coils

Chao Hu[1,2], Shuang Song[2,3], Xiaojing Wang[2], Max Q.-H. Meng[2,4], *Fellow, IEEE*, and Baopu Li[2,4]

[1]Ningbo Institute of Technology, Zhejiang University, Ningbo, Zhejiang 315100, China
[2]Shenzhen Institute of Advanced Integration Technology, Chinese Academy of Sciences/Chinese University of Hong Kong, Shenzhen Institutes of Advanced Technology, CAS, Shenzhen 518067, China
[3]Graduate School of Chinese Academy of Sciences, Yuquanlu, Beijing 100049, China
[4]The Chinese University of Hong Kong, Shatin, N.T. Hong Kong, China

The positioning and orientation system consists of three-axis generating coils and three-axis sensor coils in quasi-static magnetic field. The three-axis generating coils are fixed orthogonally and excited by the alternating current (AC) signals with different frequencies. They create the magnetic field that is equivalent to that generated by three orthogonal magnetic dipoles. Using the amplitude and phase information of the sensing signals in the sensor coils, the position and orientation parameters of the sensor coils can be computed by using an appropriate algorithm. In this paper, a novel algorithm is proposed to determine the position of the sensor coil object by some equations directly, so that its position and orientation parameters can be calculated much easier and faster. Based on this method, a system with support circuitry is designed with some special signal acquisition and sampling methods. Especially, a signal extraction (function fitting) method is proposed to pick up the coupling AC signal magnitude of the sensor coils, which simplifies the hardware circuitry and improves the signal acquisition accuracy. The simulation and real experimental results show that the system works satisfactorily with good accuracy.

***Index Terms*—Equation-based algorithm, function fitting signal extraction, positioning and orientation, three-axis magnetic dipoles.**

I. Introduction

THERE are two types of magnetic positioning and orientation techniques, which are realized by the quasi-static magnetic coils [1]–[6] and by magnets [17]–[20]. Both the techniques use magnetic dipoles as the models for the excitation sources and some magnetic sensors are used to detect the signals from the dipoles. With the coupling signals between the dipoles and sensors, the position and the orientation parameters are computed by applying some appropriate algorithms [7]–[9], [13]–[15]. The magnet dipole method has the advantages where the source dipole is power-free and easy realizable. However, the signal of the magnet is unchangeable; it must work in an environment without magnetic interferences, e.g., the medical applications as the tracking of the devices inside the human body [16], [21], [25]. On the other hand, the coil dipole method applies low-frequency AC currents to the generating coils. The sensor coils receive the specific frequency AC magnetic signals from the generating coils [3], [4], [12] so that the system can determine the position and orientation parameters on these coupling signals. This coil dipole method could have high anti-interference ability by applying appropriate signal processing methods. Therefore, the working space could be much larger and the environment constraint will not be as strict as that in magnet localization case.

Usually, the generating coils and sensing magnetic coils are arranged orthogonally, and then some specific hardware and computation methods are proposed [6]–[8], [22]–[24]. F. H. Raab *et al.* suggested using a system composed of both a three-axis magnetic-dipole source and a three-axis magnetic sensor [5]; all the source coils are excited by the same signals, then the signals of the sensors are measured and the small changes of the sensor position and orientation are determined to update the previous measurements. E. Paperno *et al.* suggest using a pair of excitation coils to generate a rotating magnetic field in space and phase quadrature, so the resulting excitation field rotates elliptically at any position in the near-field region [3]. As a result, the sensor's position and orientation can be calculated by finding the extremes of the outputs of the three-axis sensing coils. P. D. Davis *et al.* uses a pair of orthogonal magnetic sensors and found a vector of their outputs relative to the changeable magnetic field; further the magnetic object movement can be determined [22].

We also made some effort to develop an electromagnetic position and orientation system which is especially used for spinal surgery navigation [10], [11]. In our system, three orthogonal coils are used as the generating dipole object and three orthogonal coils as the sensors. In order to maintain high execution speed, all generating coils are excited simultaneously with the signals of different frequencies. The amplitudes and phases of the specific AC sensing signals are directly determined by applying a function fitting method on the sampling data; and this method not only simplifies the hardware circuitry, but also improves the signal acquisition accuracy. Then, the position and orientation of the dipole object are computed by appropriate algorithms. Here, we propose a novel algorithm that uses several mathematic equations to directly calculate the sensor position parameters relative to the generating coil center with the amplitude value and phase value of the sensing signals. Comparing with other methods which usually use matrix computation or nonlinear optimization methods, this method can calculate the

Manuscript received October 27, 2011; accepted February 06, 2012. Date of publication February 22, 2012; date of current version June 21, 2012. Corresponding author: C. Hu (e-mail: chao.hu@ciat.ac.cn).

Color versions of one or more of the figures in this paper are available online at http://ieeexplore.ieee.org.

Digital Object Identifier 10.1109/TMAG.2012.2188537

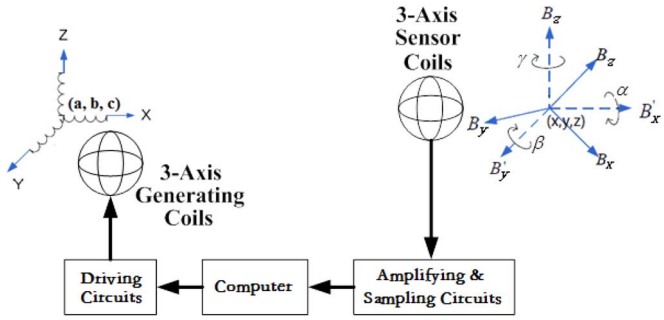

Fig. 1. System composition (three-axis generator coils and the three-axis sensor coils).

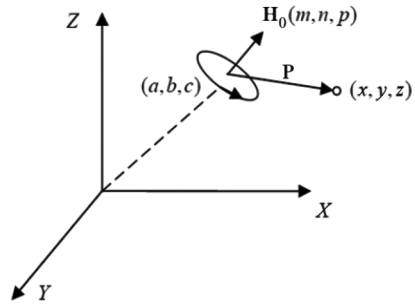

Fig. 2. Magnetic dipole model.

position and orientation parameters by some definite equations, and all the computation are realized with analytic expressions. Therefore, this method is much simpler, faster and more applicable. According to the signal acquisition method and localization algorithm, we design the electronic circuits for the signal generating and driving of the generating coils, and for the signal amplification and filtering of the receiver coils. Finally, a complete system was made and the experimental results show that the root mean square position error is about 0.6 mm and orientation error smaller than 0.3°.

The rest of this paper is organized as follows. In Section II the mathematical model of the magnetic field produced by magnetic dipole will be introduced. In Section III, the localization and orientation method will be presented. In Section IV, the hardware circuitry will be presented. In Section V, the simulation and real experiment results will be shown, followed by the conclusions in Section VI.

II. System Mathematic Model

As shown in Fig. 1, the system uses three-axis generating coils and the 3-axis sensor coils, which are along with the related electronic circuitry. The signals from the three-axis generating coils can be detected by the three-axis sensor coils by using time-sharing or frequency-coupling methods. By defining the coordinate frame, the position of the three-axis generating coils can be defined by (a, b, c); the position and orientation of the three-axis sensor coils can be defined by $(x, y, z, \alpha, \beta, \gamma)$, where (x, y, z) is the center position of the sensor coils and (α, β, γ) represents the rotation angle of the sensor coils with respect to the global coordinate frame.

A coil fed with current forms a magnetic dipole. By using the coordinate system as that in Fig. 2, the dipole's position is defined by $[a, b, c]^T$, and its direction is defined by a vector $\mathbf{H}_0(=[m, n, p]^T)$, and then the magnetic flux in a spatial position $[x, y, z]^T$ can be defined by [21]

$$\begin{aligned}\mathbf{B} &= B'_x\mathbf{i} + B'_y\mathbf{j} + B'_z\mathbf{k} \\ &= \frac{\mu_r\mu_0 M_T}{4\pi}\left(\frac{3(\mathbf{H}_0\cdot\mathbf{P})\mathbf{P}}{R^5} - \frac{\mathbf{H}_0}{R^3}\right)\end{aligned} \tag{1}$$

where B'_x, B'_y and B'_z are the three components of the magnetic flux intensity along x, y, and z axes in the spatial position $[x, y, z]^T$; μ_r is the relative permeability of the medium; μ_0 is the air magnetic permeability $(\mathrm{T}\cdot\mathrm{m/A})$; M_T is a constant defining the magnetic intensity of the dipole; $\mathbf{P}(=[x-a, y-b, z-c]^T)$ is a vector defining the spatial point $[x, y, z]^T$ with respect to the generating dipole center $[a, b, c]^T$; R is a scalar defining the length of $\mathbf{P}$ [17], [21].

III. Positioning and Orientation Method

A. Rotation Matrix

Here, we assume that the three-axis generating coils are orthogonal respectively, such that the directions of 3 generating coils are parallel to the 3 axes of the coordinate system. Also, we define B_X, B_Y and B_Z as the magnetic intensity components along the main axes of the sensing coils in the spatial position $[x, y, z]^T$, and we have

$$\mathbf{R}\begin{pmatrix} B'_x \\ B'_y \\ B'_z \end{pmatrix} = \begin{pmatrix} B_x \\ B_y \\ B_z \end{pmatrix} \tag{2}$$

where $\mathbf{R}$ is an orthonormal rotation transform matrix related to the rotation angles (α, β, γ):

$$\begin{aligned}\mathbf{R} &= Rot(z,\gamma)Rot(y,\beta)Rot(x,\alpha) \\ Rot(x,\alpha) &= \begin{pmatrix} 1 & 0 & 0 \\ 0 & \cos\alpha & -\sin\alpha \\ 0 & \sin\alpha & \cos\alpha \end{pmatrix} \\ Rot(y,\beta) &= \begin{pmatrix} \cos\beta & 0 & \sin\beta \\ 0 & 1 & 0 \\ -\sin\beta & 0 & \cos\beta \end{pmatrix} \\ Rot(z,\gamma) &= \begin{pmatrix} \cos\gamma & -\sin\gamma & 0 \\ \sin\gamma & \cos\gamma & 0 \\ 0 & 0 & 1 \end{pmatrix}.\end{aligned} \tag{3}$$

According to (1), we have

$$\begin{cases} B'_x = B_T\left\{\frac{3[m(x-a)+n(y-b)+p(z-c)](x-a)}{R^5} - \frac{m}{R^3}\right\} \\ B'_y = B_T\left\{\frac{3[m(x-a)+n(y-b)+p(z-c)](y-b)}{R^5} - \frac{n}{R^3}\right\} \\ B'_z = B_T\left\{\frac{3[m(x-a)+n(y-b)+p(z-c)](z-c)}{R^5} - \frac{p}{R^3}\right\} \end{cases} \tag{4}$$

where

$$B_T = \mu_r\mu_0 M_T/4\pi,\ R = \sqrt{(x-a)^2+(y-b)^2+(z-c)^2}.$$

Since the magnetic signals made by each coil of the three-axis generating coils can be detected independently, we can derive the following equations.

Fix the coil-I with its main axis parallel to the x-axis, we get $(m, n, p) = (1, 0, 0)$. From (4), we have

$$B'_{x1} = B_T \left(\frac{3(x-a)^2}{R^5} - \frac{1}{R^3} \right) \tag{5}$$

$$B'_{y1} = B_T \frac{3(x-a)(y-b)}{R^5} \tag{6}$$

$$B'_{z1} = B_T \frac{3(x-a)(z-b)}{R^5}. \tag{7}$$

Fix the coil-II with its main axis parallel to the y-axis, we get $(m, n, p) = (0, 1, 0)$, and we have

$$B'_{x2} = B_T \frac{3(x-a)(y-b)}{R^5} \tag{8}$$

$$B'_{y2} = B_T \left(\frac{3(y-b)^2}{R^5} - \frac{1}{R^3} \right) \tag{9}$$

$$B'_{z2} = B_T \frac{3(y-b)(z-c)}{R^5}. \tag{10}$$

Fix the coil-III with its main axis parallel to the z-axis, we get $(m, n, p) = (0, 1, 0)$, and we have

$$B'_{x3} = B_T \frac{3(x-a)(z-c)}{R^5} \tag{11}$$

$$B'_{z3} = B_T \frac{3(y-b)(z-c)}{R^5} \tag{12}$$

$$B'_{y3} = B_T \left(\frac{3(z-c)^2}{R^5} - \frac{1}{R^3} \right). \tag{13}$$

B. Equation-Based Algorithm

Because the rotation transform matrix $\mathbf{R}$ in (2) is orthonormal, we have

$$B'^{\,2}_x + B'^{\,2}_y + B'^{\,2}_z = B^2_x + B^2_y + B^2_z. \tag{14}$$

To simplify the problem, let $(a, b, c) = (0, 0, 0)$. For generating coil I, from (5)–(7), we have the magnetic flux:

$$\begin{aligned} B_1^2 &= B_{x1}{}^2 + B_{y1}{}^2 + B_{z1}{}^2 = B'_{x1}{}^2 + B'_{y1}{}^2 + B'_{z1}{}^2 \\ &= B_T^2 \left(\frac{3x^2}{R^8} + \frac{1}{R^6} \right). \end{aligned} \tag{15}$$

Similarly, for Coil II and III, we have

$$\begin{aligned} B_2^2 &= B_{x2}{}^2 + B_{y2}{}^2 + B_{z2}{}^2 = B'_{x2}{}^2 + B'_{y2}{}^2 + B'_{z2}{}^2 \\ &= B_T^2 \left(\frac{3y^2}{R^8} + \frac{1}{R^6} \right) \end{aligned} \tag{16}$$

$$\begin{aligned} B_3^2 &= B_{x3}{}^2 + B_{y3}{}^2 + B_{z3}{}^2 = B'_{x3}{}^2 + B'_{y3}{}^2 + B'_{z3}{}^2 \\ &= B_T^2 \left(\frac{3z^2}{R^8} + \frac{1}{R^6} \right). \end{aligned} \tag{17}$$

TABLE I
SIGN DETERMINATION OF THE POSITION PARAMETERS

B_{12} B_{13} B_{23}	x y z
+ + +	+ + + / - - -
+ + -	**Not Existing**
+ - +	**Not Existing**
+ - -	- - + / + + -
- + +	**Not Existing**
- + -	+ - + / - + -
- - +	- + + / + - -
- - -	**Not Existing**

Sum them up, we have

$$B^2 = \sum_{i=1,2,3} B_i^2 = \frac{6B_T^2}{R^6} \tag{18}$$

and

$$R = \sqrt[6]{\frac{6B_T^2}{B^2}}. \tag{19}$$

Back to (15), (16) and (17), we have

$$x = \pm \frac{\sqrt{B_1^2/B_T^2 - B^2/(6B_T^2)}}{\sqrt{3}\left[B^2/(6B_T^2)\right]^{\frac{2}{3}}} \tag{20}$$

$$y = \pm \frac{\sqrt{B_2^2/B_T^2 - B^2/(6B_T^2)}}{\sqrt{3}\left[B^2/(6B_T^2)\right]^{\frac{2}{3}}} \tag{21}$$

$$z = \pm \frac{\sqrt{B_3^2/B_T^2 - B^2/(6B_T^2)}}{\sqrt{3}\left[B^2/(6B_T^2)\right]^{\frac{2}{3}}}. \tag{22}$$

Now, we need to find the signs of the x, y, and z. From (2), we know that the inner product $\vec{\mathbf{B}}'_i \bullet \vec{\mathbf{B}}'_j = \vec{\mathbf{B}}_i \bullet \vec{\mathbf{B}}_j$ $(i = 1, 2, 3;\ j = 1, 2, 3)$; so we have

$$\frac{3B_T}{R^6} xy = B_{x1}B_{x2} + B_{y1}B_{y2} + B_{z1}B_{z2} = B_{12}$$

$$\frac{3B_T}{R^6} xz = B_{x1}B_{x3} + B_{y1}B_{y3} + B_{z1}B_{z3} = B_{13}$$

$$\frac{3B_T}{R^6} yz = B_{x2}B_{x3} + B_{y2}B_{y3} + B_{z2}B_{z3} = B_{23}.$$

Then, the signs of x, y, z can be determined as in Table I. For example, when the signs of (B_{12}, B_{13}, B_{23}) are $(+\,-\,-)$, the signs of (x, y, z) will be $(-\,-\,+)$ or $(+\,+\,-)$; when the signs of (B_{12}, B_{13}, B_{23}) are $(+\,+\,-)$, no (x, y, z) matches it. In real application, we can also use sequential message to determine

TABLE II
EXECUTION TIME (MS) FOR DIFFERENT INITIAL GUESS ERROR (ALL THE SAMPLES HAVING THE COMPUTATION ERROR < 0.1 MM)

IG-Error(mm)	5	25	50	100	150	250	350	500	900
LM	32.2	36.5	40.2	42.9	44.5	45.7	46.7	48.0	50.1
Eq.+LM	32.5	32.5	32.1	33.1	32.6	32.5	32.4	32.7	32.8

these signs; define the one axis to be positive so that the solution will be unique.

With (x, y, z), B'_x, B'_y and B'_z can be calculated with (4), then the rotation matrix $\mathbf{R}$ can be determined by the sampled data ($B_{\mathrm{xi}}, B_{\mathrm{yi}}, B_{\mathrm{zi}}; i = 1, 2, 3$) of the three-axis sensor coils as (2)

$$R\begin{pmatrix} B'_{x1} & B'_{x2} & B'_{x3} \\ B'_{y1} & B'_{y2} & B'_{y3} \\ B'_{z1} & B'_{z2} & B'_{z3} \end{pmatrix} = \begin{pmatrix} B_{x1} & B_{x2} & B_{x3} \\ B_{y2} & B_{y2} & B_{y3} \\ B_{z1} & B_{z2} & B_{z3} \end{pmatrix}$$

$$R = \begin{pmatrix} B_{x1} & B_{x2} & B_{x3} \\ B_{y2} & B_{y2} & B_{y3} \\ B_{z1} & B_{z2} & B_{z3} \end{pmatrix} \times \begin{pmatrix} B'_{x1} & B'_{x2} & B'_{x3} \\ B'_{y1} & B'_{y2} & B'_{y3} \\ B'_{z1} & B'_{z2} & B'_{z3} \end{pmatrix}^{-1}. \quad (23)$$

So the position and orientation of the object are all determined.

C. Nonlinear Optimization Algorithm

From (2)–(4), we know that B'_{xi}, B'_{yi}, and B'_{zi} are the function of the sensor position parameters (x, y, z) and orientation parameters (α, β, γ). We obtain three equations for each generating coil and three-axis sensor coils. Since there are six position and orientation parameters $(\mathrm{x}, \mathrm{y}, \mathrm{z}, \alpha, \beta, \gamma)$, two single-axis generating coils is the minimal to solve the six unknown parameters. In order to improve the accuracy, more generating coils are preferable, on the condition that all the signals can be sampled within a satisfactory time period.

Assume that three-axis generating coils are arranged in the positions (a_{ji}, b_{ji}, c_{ji}) (where $i = 1, 2, 3$, referred to the three-axes; $j = 1, 2, \ldots M$, referred to the number of the three-axis generating coils). To simplify the problem, the orientations (m_{ji}, n_{ji}, p_{ji}) for all three-axis generating coils are fixed in the same direction, in which the three orientation vectors of the coils are (1, 0, 0), (0, 1, 0) and (0, 0, 1); Then, we have nine equations as the (5)–(13) for each pair of three-axis generating coils and three-axis sensor coils. Define

$$\mathrm{E}_{ji} = \begin{pmatrix} B_{jxi} - \mathrm{R}_{j1}B'_{jxi} \\ B_{jyi} - \mathrm{R}_{j2}B'_{jyi} \\ B_{jzi} - \mathrm{R}_{j3}B'_{jzi} \end{pmatrix} (i = 1, 2, 3; j = 1, 2, \ldots M) \quad (24)$$

where B_{jxi}, B_{jyi}, and B_{jzi} refer to the sampled magnetic intensities of the three-axis sensor coils (defined as x, y, and z) in position (x, y, z) with respect to the ith axis coil ($i = 1, 2, 3$) of the jth generating (three-axis) coil ($j = 1, 2, \ldots, M$). R_{j1}, R_{j2}, and R_{j3} are the 1st, 2nd, and 3rd row of the rotation matrix R_j corresponding to the jth generating (three-axis) coil. With (24), we define error objective function as

$$\Lambda = \sum_{j=1}^{M} \left(\mathbf{E}_{j1}^T \mathbf{E}_{j1} + \mathbf{E}_{j2}^T \mathbf{E}_{j2} + \mathbf{E}_{j3}^T \mathbf{E}_{j3} \right). \quad (25)$$

Now, we need find the optimal parameters $(x, y, z, \alpha, \beta, \gamma)$ to minimize Λ. This is an optimization problem and with redundant messages if there are more than two three-axis generating coils. There are several methods can be used to solve this problem [18]–[21]. Through the trials, we found that Levenberg-Marquardt (LM) method has good calculation accuracy and robustness [26].

However, comparing with the equation-based method, the LM method has lower execution speed and might fail to give correct solution when the initial guess of the parameters has large errors. To address this problem, we propose a novel algorithm combining these two algorithms. There, the equation-based algorithm is first used to find the localization and orientation parameters, and then the nonlinear algorithm is applied for further computation by using the initial parameters obtained from the equation-based algorithm. Since these initial parameters are very close to those globally true position and orientation parameters, the nonlinear algorithm can be easily convergent to correct solution. As a result, the system has both the satisfactory localization accuracy and time efficiency. As shown in Table II, we tested the algorithm for 50 times for each initial guess errors (IG-Error) from $5 \sim 900$ mm; and all the samples have the computation error < 0.1 mm. The execution time of LM algorithm increase with the initial guess error, while the equation-based and LM algorithm (Eq. $+$LM) has very closed results around 32 mS. Also we found three fails for LM algorithm in initial guess error $= 900$ mm.

IV. SYSTEM COMPOSITION AND SIGNAL SAMPLING

A. Circuit System

Fig. 3 shows the system and circuit PCB. The system (Fig. 4 shows the block diagram) is composed of the generator part and receiver part. For the generator part, sine AC signal with specific frequency is produced by MAX038 (Product of U.S. Maxim Company) and powered by a power amplifier LM3886 (U.S. NS Company Product). The three-axis generating coil probe (as shown in Fig. 5(a)) has outer size $5\ \mathrm{cm} \times 5\ \mathrm{cm} \times 5\ \mathrm{cm}$ with each coil of 300 turns. They are excited by this circuit and their outputs can be switched on or off by the work station through the digital output ports.

For the receiver (or sensor) part, the AC signals are induced by the sensor coils corresponding to the magnetic flux signals from the generator coils (as shown in Fig. 5(b)). Its outer size

Fig. 3. System PCB.

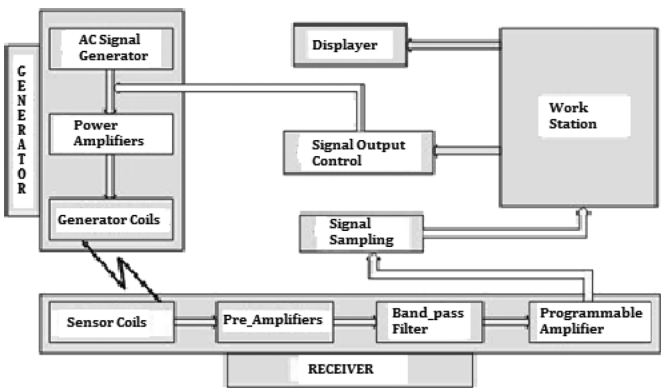

Fig. 4. Circuit system composition.

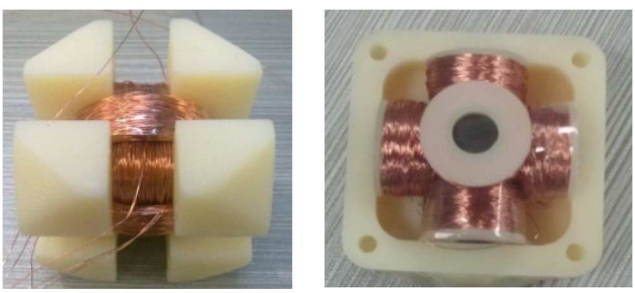

(a) (b)

Fig. 5. Generating and sensor coils. (a) Generating coils; (b) Sensor coils.

is 3 cm × 3 cm × 3 cm, and each coil has 1600 turns with a ferromagnetic core to strengthen the magnetic signals. Then the signal is amplified by a pre-amplifier, and the specific frequency magnetic coupling signal is processed by a band filter. Then the work station samples the signals from the sensor coils through the analog to digital converter (ADC). In order to meet the voltage range (±5 V) of the signal sampling ADC card (PCI-1730U, Advantech, Taiwan), a programmable amplifier is used for different amplifications for different ranges of the magnetic coupling signals.

B. Signal Extraction Method

To guarantee the precision of the position and orientation, the most important step is to extract the output voltage as accurately as possible. Because the large scope of the moving object, the signal could be very weak, so a high quality amplifying and filtering circuit and an appropriate signal extraction method must be found [11].

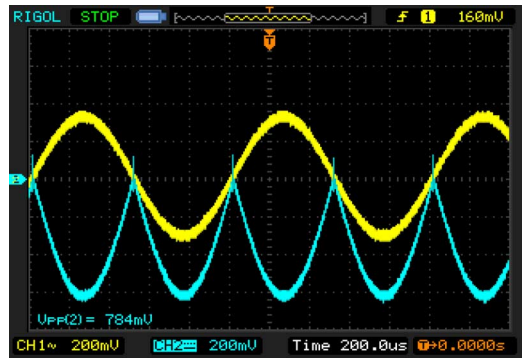

Fig. 6. Lock amplifier output with reference $Phase = \pi$.

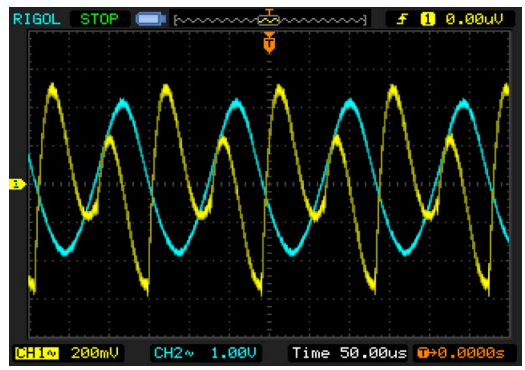

Fig. 7. Lock amplifier output with reference $Phase \neq 0$ or π.

1) Extracting Signal by Phase Lock Amplifier: To obtain the magnetic coupling signal intensity, a phase lock amplifier is used to change the AC signal to DC signal with respect to the reference signal. In our system, it is made of an amplifier AD630 and a low-pass filter. AD630 has two inputs: the signal input and reference. The reference signal plays a role as a selecting switch. When it is positive, the signal passes it directly; when it is negative, the signal passes through it inversely. The low-pass filter is used to pick up the DC component of the output of the lock amplifier AD630, which is proportional to the amplitude of the input signal. Fig. 6 and Fig. 7 show the outputs of AD 630 with respect to different references, where the yellow curve is the input and blue curve the output of the AD630. We observe that the outputs are different with different reference phases, and the ideal one is that the reference $phase = 0$, or π with respect to that of the input signal.

In order to maintain equivalent amplification for different amplitudes of the inputs, we must fix the phase of the lock amplifier and the ideal reference is having the same (or inverse) phase as that of the input signal (as Fig. 6). However, in the real circuitry, we found that it is very difficult to maintain this condition, and the phase of the input signal changes in some extent with respect to that of the reference signal, so that the accuracy might not be so desirable.

2) Extracting Signal by Function Fitting: Here, we propose a method by extracting the amplitude of the sampling signal of the AC coupling signal instead of that of the phase lock amplifier. The system directly samples the AC signals from the sensor coils through the ADCs after sensor signals are amplified and filtered. When the work station accepts enough data, a function fitting method is applied to extract the signal at the definite transmitting frequency.

Suppose an AC signal is $e = A{*}sin(wt + \varphi) + c$ and we rewrite it as

$$e = a{*}sin(wt) + b{*}cos(wt) + c \tag{26}$$

Sample the signal, and we get

$$e(i) = a{*}sin(wt_i) + b{*}cos(wt_i) + c \tag{27}$$

Where $i = 1, 2, \ldots$. The function $e(i)$ fits the sampled signal e_i by the least square method; and we get the following equation:

$$\begin{pmatrix} \sum_{i=1}^{n}\sin^2(wt_i) & \sum_{i=1}^{n}(\sin(wt){*}\cos(wt_i)) & \sum_{i=1}^{n}\sin(wt_i) \\ \sum_{i=1}^{n}(\sin(wt){*}\cos(wt)) & \sum_{i=1}^{n}\cos^2(wt_i) & \sum_{i=1}^{n}\cos(w_i) \\ \sum_{i=1}^{n}\sin(wt_i) & \sum_{i=1}^{n}\cos(wt_i) & \sum_{i=1}^{n}1 \end{pmatrix} * \begin{bmatrix} \mathrm{a} \\ \mathrm{b} \\ \mathrm{c} \end{bmatrix} = \begin{bmatrix} \sum_{i=1}^{n}(e_i{*}\sin(wt)) \\ \sum_{i=1}^{n}(e_i{*}\cos(wt)) \\ \sum_{i=1}^{n} e_i \end{bmatrix}$$

Solve it, we get a, b, and c. We use $A = \sqrt{a^2 + b^2}$ to represent the amplitude of the signal (coil signal is in AC, so the constant c does not affect the receiving signal and is ignored). A is proportional to magnetic intensity in the specific spatial position, and its real value can be computed through the coupling sensitivity of the receiving coil corresponding to the specific generating coil, while the sensitivity can be determined by the calibration process.

This function fitting method does not have the step of the phase lock amplification, so that it has higher precision. The drawback is that it must acquire enough data for high accuracy, such that the execution speed might be affected. So we must find a fast ADC sampling circuit and fast switch controls on the different sensor coil samples.

V. Performance Evaluation

In this section, the performance of the proposed method is evaluated by using simulation experiment.

A. Function Fitting Evaluation

Fig. 8 shows the output signal amplitudes that the signal with frequency 70 fits different frequency 80, 10, 130, 130, and phases 51.34°, 51.34°, 51.34°, 38.66°. We observe that the resulted output error of the fitting is decreased with the samples increase and approach to zero when samples increase to infinity.

Fig. 9 shows the output signal amplitudes that one signal with frequency 70 fits with different input signals with noise frequencies. The curve 1 in red has the signal with 70 Hz only. The curve 2 in blue has the signal:

$$\mathrm{S1} = 4\sin(2\pi * 70) + 5\cos(2\pi * 70) + 3\sin(2\pi * 10\mathrm{n}) + 5\cos(2\pi * 10\mathrm{n}) + 1);$$

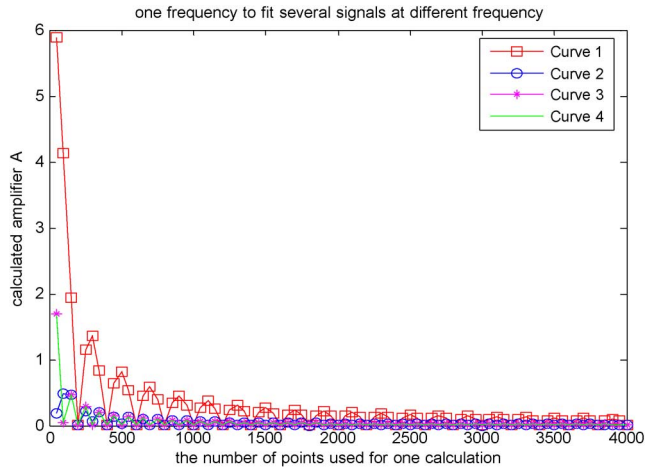

Fig. 8. Fitting with different frequency signal (The fitting frequency $f = 70$, the frequencies of the input signals in Curve 1, 2, 3, 4 are 80, 10, 130, 130 and phases 51.34°, 51.34°, 51.34°, 38.66°).

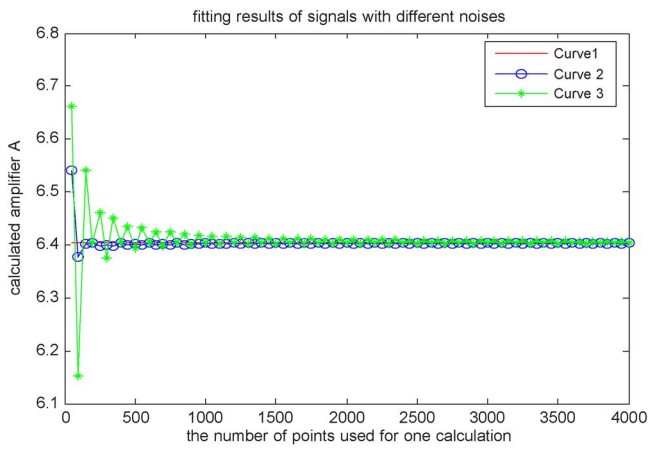

Fig. 9. Fitting signal with 70 Hz with signals with noises. Curve 1 (red): has the signal with 70 Hz only; Curve 2 (blue): $\mathrm{S1} = 4\sin(2\pi * 70) + 5\cos(2\pi * 70) + 3\sin(2\pi * 10\mathrm{n}) + 5\cos(2\pi * 10\mathrm{n}) + 1)$. Curve 3 (green): $\mathrm{S2} = 4\sin(2\pi * 70) + 5\cos(2\pi * 70) + 3\sin(2\pi * 130\mathrm{n}) + 5\cos(2\pi * 130n) + 1)$.

The Curve 3 in green has the signal:

$$\mathrm{S2} = 4\sin(2\pi * 70) + 5\cos(2\pi * 70) + 3\sin(2\pi * 130\mathrm{n}) + 5\cos(2\pi * 130\mathrm{n}) + 1.$$

We observe

1) There is no fitting error when the input signal frequency is the same as that of the fitting signal (as Curve-1).
2) The larger frequency difference of the fitting signal and the noise signal, the smaller the fitting error.
3) The fitting error signal decreases with sample number periodically.

B. Positioning and Orientation Algorithm Evaluation

The algorithm was tested in MATLAB programs, and the magnetic intensities of the three-axis sensing coils are created in uniformly predetermined positions and directions in a space of 1 m $*$ m $*$ 1 m. The position of the three-axis generator is fixed in $(a, b, c) = (0, 0, 0)$.

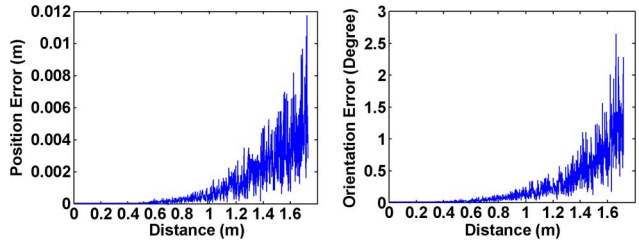

Fig. 10. Localization & Orientation errors with distance in a space of $1\ \mathrm{m}^{*}1\ \mathrm{m}^{*}1\ \mathrm{m}$ at the noise level $0.001(^{*}\mathrm{Bt})$.

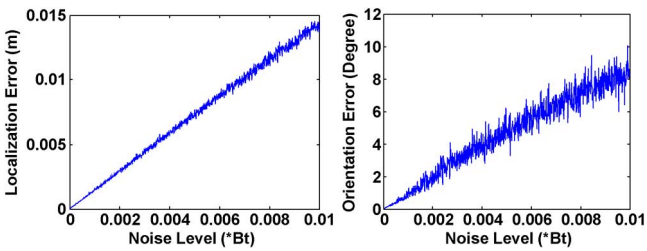

Fig. 11. Localization & orientation errors with noise level.

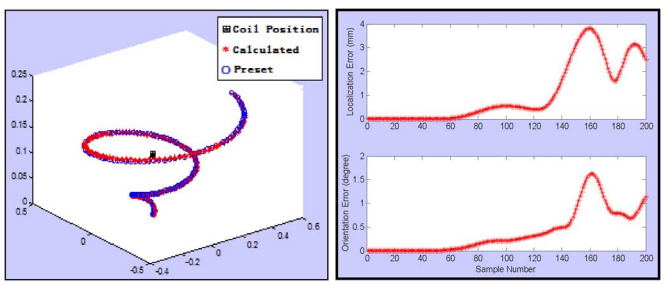

Fig. 12. Errors for tracking helix locus with $\mathrm{SNR} = 10:1$. Three-axis coils are placed in (0, 0, 0.12 m).

In order to test the anti-interference ability of the method, white-noises are added in the sensor signals. To evaluate the performances, we define the localization error and the orientation error to be

$$E_p = \sqrt{(x_c - x_r)^2 + (y_c - y_r)^2 + (z_c - z_r)^2} \quad (28)$$

$$E_o = |\alpha_c - \alpha_r| + |\beta_c - \beta_r| + |\gamma_c - \gamma_r| \quad (29)$$

where $(x_r, y_r, z_r, \alpha_r, \beta_r, \gamma_r)$ is the predefined position and orientation; $(x_c, y_c, z_c, \alpha_c, \beta_c, \gamma_c)$ is the calculated result with the proposed method.

Fig. 10 shows simulation results of the localization error and orientation error at the noise level $0.001(^{*}\mathrm{Bt})$. Fig. 11 shows the position error and orientation error with the noise level range from 0 $(^{*}\mathrm{Bt})$ to $0.01(^{*}\mathrm{Bt})$. From the results, we observe that the error increases with the noises; when the noise level is low $(< 0.002^{*}\mathrm{Bt})$ and the distance between sensor and generator is not far (<1.2 m), the localization and orientation method can have a good performance with localization error about $1 \sim 2$ mm and orientation error about $0.37 \sim 0.4°$.

Fig. 12 shows localization property for the system to track a helix locus, where the three-axis coils are placed in (0, 0, 0.12 m) and the signal-noise ratio is 10:1. We observe that the tracking errors are within several millimeters when the receiver moves in the space of (x:−0.5:0.5 m), (y:−0.4:0.6 m) and (z: 0:0.25 m).

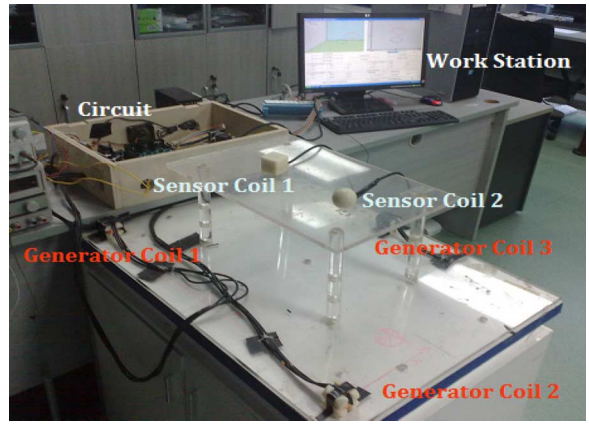

Fig. 13. Test system.

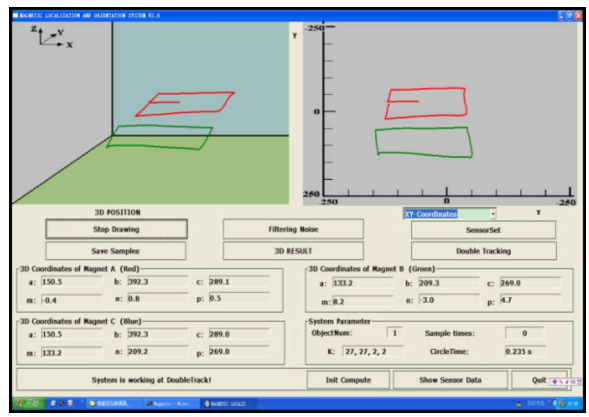

Fig. 14. Interface for real time tracking system.

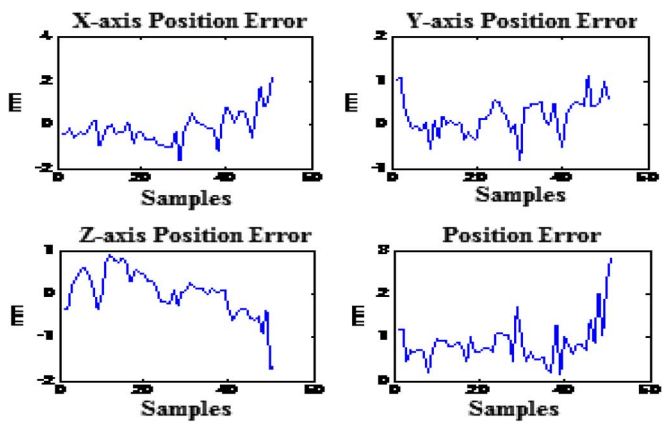

Fig. 15. Position errors.

C. Real System Evaluation

We built the real tracking system with three three-axis generating coils and two three-axis sensor coils as shown in Fig. 13. The real-time tracking was realized by the work station through the amplification and sampling circuits. Fig. 14 shows the interface for real time tracking. It can display the 2-D/3-D tracking locus and the position and orientation parameters for 1 to 3 objects. The samples are uniformly distributed in the space of $500\ \mathrm{mm} \times 400\mathrm{mm} \times 400\ \mathrm{mm}$ as shown in Fig. 17 and test results shown in Figs. 15–17.

We observe that the position error changes within 2 mm in each axis and the average error is around 1 mm. The average orientation error is smaller than 1°. The stability was also tested

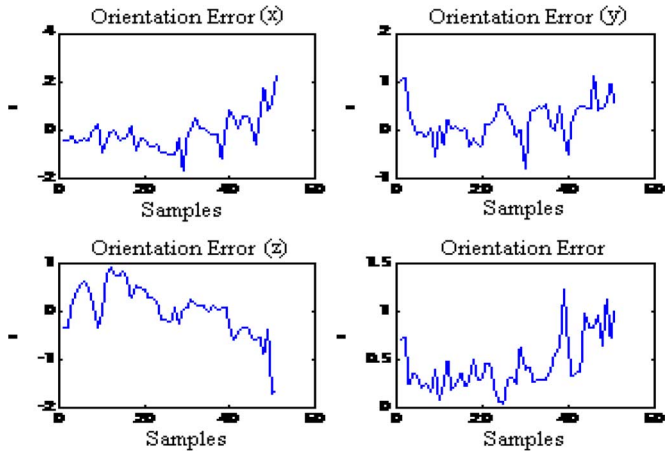

Fig. 16. Orientation errors.

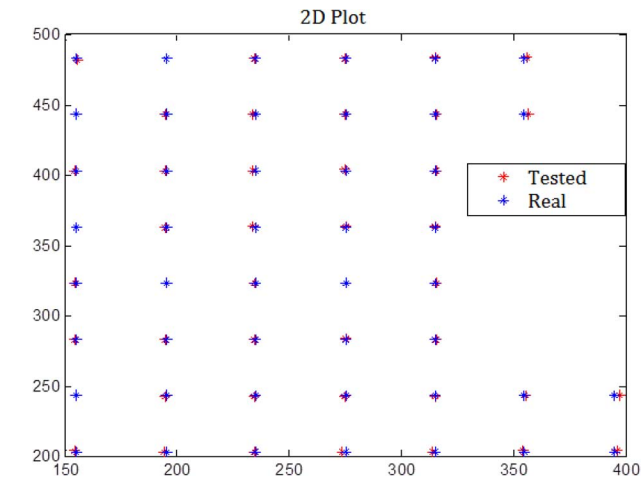

Fig. 17. 2-D position plot (mm).

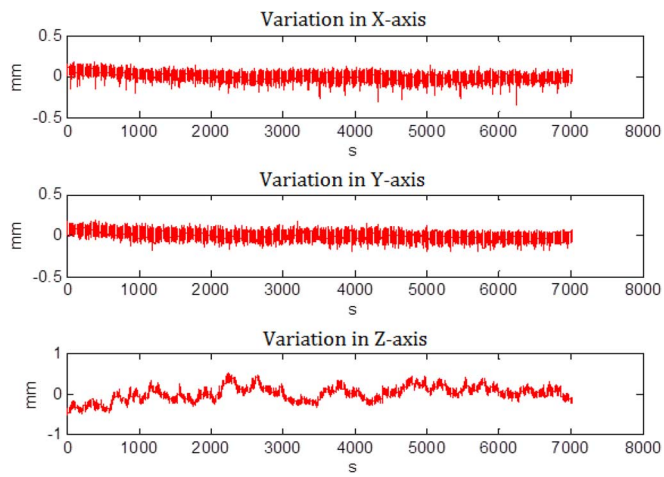

Fig. 18. Position error variation in time period of 7000 s.

and Fig. 18 shows the variations of the position errors within 0.5 mm in time duration of 7000 s.

Table III shows the mean errors and the mean square errors for the position and orientation. We observe that the absolute mean position error is 0.87 mm and the absolute mean orientation error is 0.64°; while the root mean square error position error is 0.60 mm and the mean orientation error is 0.26°. This accuracy is comparative to that of the other commercial products of the electromagnetic positioning systems; e.g., NDI has several types of Aurora electromagnetic measurement systems; the root mean square position error is about 0.80 to 1.1 mm, and the root mean orientation error is about 0.15° to 0.20°; the electromagnetic positioning system "trakSTAR 2" of Ascension Technology Corporation has the root mean square position error is about 1.4 mm, and the root mean square orientation error is about 0.5°.

TABLE III
POSITION AND ORIENTATION ERRORS

	Absolute Mean	Root Mean Square
x	0.54 mm	0.50 mm
y	0.35 mm	0.16 mm
z	0.41 mm	0.30 mm
Total	0.87 mm	0.60 mm
α	0.17°	0.043°
β	0.17°	0.045°
γ	0.30°	0.173°
Total	0.64°	0.26°

VI. CONCLUSION

The electromagnetic localization and orientation system uses three orthogonal generating coils and three orthogonal sensor coils. To obtain high precision magnetic intensity signals, a special function fitting method is proposed based on the AC coupling signals between the generating and sensor coils, which makes the hardware circuit simpler. Then, based on the three-axis magnetic dipole model, a novel localization and orientation algorithm is proposed that uses several mathematic equations to directly calculate the position and orientation parameters of the object, and these parameters are optimized with LM method. Comparing with other techniques, this method is much simpler, faster and more applicable. Finally, a complete system is designed and realized with the specific generating and sensing circuits. The real experimental results show that the positioning accuracy is within 1 mm and orientation accuracy is within 0.7°.

ACKNOWLEDGMENT

This work was supported by the San-Jiang Scholar Supporting Fund from Ningbo Institute of Technology/Zhejiang University, the grants from National Sci. & Tech. Pillar Program (2008BAI65B21), Guangdong/CAS Cooperation Project (2009B091300160), and the National Natural Science Foundation (60904031).

REFERENCES

[1] NDI Aurora Electromagnetic Tracking System [Online]. Available: http://www.ndigital.com/aurora.php
[2] Ascension Tech. Corporation Products Appl. [Online]. Available: http://www.ascension-tech.com/products/microbird.php
[3] E. Paperno, I. Sasada, and E. Leonovich, "A new method for magentic position and orientation tracking," *IEEE Trans. Magn.*, vol. 37, no. 4, pp. 1938–1940, Jul. 2001.
[4] H. P. Kalmus, "A new guiding and tracking system," *IRE Trans. Aerosp. Nav. Electron.*, vol. 9, pp. 7–10, 1962.

[5] F. H. Raab, E. B. Blood, T. O. Steiner, and H. R. Jones, "Magnetic position and orientation tracking system," *IEEE Trans. Aerosp. Electron. Syst.*, vol. AES-15, no. 5, pp. 709–717, 1979.

[6] J. Kuipers, "Apparatus for Generating a Nutating Electromagnetic Field," U.S. Patent 40170858, Apr. 1977.

[7] P. K. Hansen, "Method and Apparatus for Position and Orientation Measurement Using a Magnetic Field and Retransmission," U.S. Patent 4642786, Feb. 1987.

[8] F. H. Raab, "Remote Object and Orientation Locator," U.S. Patent 4315251, Feb. 1982.

[9] T. Nara, S. Suzuki, and S. Ando, "A closed-form formula for magnetic dipole localization by measurement of its magnetic field and spatial gradients," *IEEE Trans. Magn.*, vol. 42, no. 10, pp. 3291–3293, Oct. 2006.

[10] M. Li, S. Song, C. Hu, D. M. Chen, and M. Q.-H. Meng, "A novel method of 6-DoF electromagnetic navigation system for surgical robot," in *Proc. 8th World Congress on Intelligent Control and Automation*, Jinan, China, Jul. 2010, pp. 2163–2167.

[11] X. J. Wang, S. Song, and C. Hu, "The extraction technology of week coupling AC signal in an electromagnetic localization system," in *2010 IEEE Int. Conf. Robotics and Biomimetics*, Tianjin, China, Dec. 2010, pp. 170–1175.

[12] A. Plotkin, E. Paperno, G. Vasserman, and R. Segev, "Magnetic tracking of eye motion in small, fast-moving animals," *IEEE Trans. Magn.*, vol. 44, no. 11, pp. 4492–4495, Nov. 2008.

[13] Y. Barrell and H. W. L. Naus, "Detection and localisation of magnetic objects," *IET Sci. Meas. Technol.*, vol. 1, no. 5, pp. 245–254, 2007.

[14] L. Vaizer, J. Lathrop, and J. Bono, "Localization of magnetic dipole targets," in *Proc. MTTS/IEEE TECHNO-OCEAN'04*, Panama City, FL, Nov. 2004, pp. 869–873.

[15] W. M. Wynn, "Magnetic dipole localization with a gradiometer: Obtaining unique solutions," in *1997 Int. Geoscience and Remote Sensing Symposium: Remote Sensing-A Scientific Vision for Sustainable Development*, Singapore, Aug. 1997, pp. 1483–1485.

[16] J. A. Baldoni and B. B. Yellen, "Magnetic tracking system: monitoring heart valve prostheses," *IEEE Trans. Magn.*, vol. 43, no. 6, pp. 2430–2432, Jun. 2007.

[17] C. Hu, M. Q.-H. Meng, and M. Mandal, "A linear algorithm for tracing magnet's position and orientation by using 3-axis magnetic sensors," *IEEE Trans. Magn.*, vol. 43, no. 12, pp. 4096–4101, Dec. 2007.

[18] W. A. Yang, C. Hu, M. Li, M. Q.-H. Meng, and S. Song, "A new tracking system for three magnetic objectives," *IEEE Trans. Magn.*, vol. 46, no. 12, pp. 4023–4029, Dec. 2010.

[19] C. Hu, M. Li, S. Song, W. A. Yang, R. Zhang, and M. Q.-H. Meng, "A cubic 3-axis magnetic sensor array for wirelessly tracking magnet position and orientation," *IEEE Sensors J.*, vol. 10, no. 5, pp. 903–913, May 2010.

[20] W. A. Yang, C. Hu, M. Q.-H. Meng, S. Song, and H. D. Dai, "A six-dimensional magnetic localization algorithm for a rectangular magnet objective based on a particle swarm optimizer," *IEEE Trans. Magn.*, vol. 45, no. 8, pp. 3092–3099, Aug. 2009.

[21] C. Hu, M. Q.-H. Meng, and M. Mandal, "Efficient magnetic localization and orientation technique for capsule endoscopy," *Int. J. Inform. Acquisition*, vol. 2, no. 1, pp. 23–36, 2005.

[22] P. D. Davis, J. Garland, T. E. McCullough, and Dallas, "Magnetic Detection System For Detection Movement of an Object Utilizing Signals Derived from Two Orthogonal Pickup Coils," U.S. Patent 3644825, Feb. 22, 1972.

[23] D. D. Frantz, A. D. Wiles, S. E. Leis, and S. R. Kirsch, "Accuracy assessment protocols for electromagnetic tracking systems," *Phys. Med. Biol.*, vol. 48, pp. 2241–2251, 2003.

[24] J. Hummel, M. Figl, C. Kollmann, and H. Bergmann, "Evaluation of a miniature electro-magnetic position tracker," *Med. Phys.*, vol. 29, no. 10, pp. 2205–2212, 2002.

[25] W. Andra, H. Danan, W. Kirmße, H.-H. Kramer, P. Saupe, R. Schmieg, and M. E. Bellemann, "A novel method for real- time magnetic marker monitoring in the gastrointestinal tract," *Phys. Med. Biol.*, vol. 45, pp. 3081–3093, 2000.

[26] A. Ranganath, The Levenberg-Marquardt Algorithm, June 8, 2004.